PIER M

(Received 20 December 2023, Accepted 5 February 2024, Scheduled 21 February 2024)

A Low SAR High Isolation Fully Flexible MIMO Antenna Integrated with AMC Array

Ling Zhang, Cheng-Zhu Du*, Hai-Feng Shu, and Zhi-Hua Yue

College of Electronics and Information Engineering, Shanghai University of Electric Power, Shanghai 200090, China

ABSTRACT: This paper presents a flexible wearable multiple-input multiple-output (MIMO) antenna with low specific absorption rate (SAR) and high isolation based on artificial magnetic conductor (AMC), which is applied to wireless body area network (WBAN). The antenna consists of two orthogonal antenna elements, which are connected to the ground, and the size is 45 mm $\times$ 22 mm $\times$ 0.1 mm. By integrating a 4×5 square artificial magnetic conductor array on the back of the antenna, the gain of the antenna is improved, and the backward radiation of the antenna to the human body is reduced. Both antenna and AMC array are printed on 0.1 mm flexible substrate liquid crystal polymer (LCP). The results of measurement illustrate that the integrated antenna operates at 5.55 GHz–6.4 GHz (14.6%), and the port isolation is better than 20 dB. At 5.8 GHz, the measured antenna gain is 7.92 dBi, and the front-to-back ratio (FBR) is 17.5 dB. The analysis results of integrated antenna placement at different parts of the human body and bending measurement show that the SAR value is reduced by 99.4%, and the measured performance is good. The proposed MIMO antenna integrated with AMC can be safely applied in wearable applications.

1. INTRODUCTION

With wearable devices progressing rapidly, scholars are increasingly focusing their attention on research related to wireless body area networks (WBANs). There are numerous applications for WBANs in our daily lives. They are used in the healthcare industry, such as glucose monitoring systems and blood pressure monitors, to monitor a patient's serious medical condition. They can also be used in emergency and rescue response systems, as well as in the entertainment, military, commercial, and rescue industries, and integrated into shoes, jackets, raincoats, and helmets [1].

The performance of the antenna will be impacted by the substrate made from various materials [2]. The permittivity and thickness of the substrate play a significant role in determining the bandwidth and efficiency of a planar microstrip antenna [3]. Due to the development of wearable antennas, the research on patch antennas has mostly focused on flexible materials [4–15]. At present, wearable antennas extensively use various textile materials as the substrate, including felt [4, 8, 10, 14], jeans [9, 11], and some other flexible materials like leather [13]. The purpose of using these flexible materials is to achieve better integration of the antenna and conformal with the human body.

Wearable antennas are a hot spot for current researchers. The antenna performances of high gain and low specific absorption ratio (SAR) are important evaluation metrics, and the metamaterial structure is used to improve the antenna performances [4–7, 8–16]. Wearable antennas can be applied to healthcare fields, such as brainwave meter, electrocardiogram monitor, and defibrillator. In the military field, it can be integrated into helmet or clothing of soldier to locate the soldier's position and convey military information. When the wearable antenna is backed on an artificial magnetic conductor (AMC) structure, the radiation from the back lobes is reduced effectively; the SAR value of the antennas towards the human is exceptionally low, and at the same time, the antennas obtain high gain.

In [8], a foldable dipole antenna based on AMC is proposed for health monitoring, with a SAR value of only 0.0091 W/kg, while achieving a gain improvement of 5.16 dBi. In [10], the antenna backed with 3×3 AMC array obtains a gain of 5 dBi and 99.9% reduction in backward radiation towards the human body. In [12], a forward gain of 7.47 dBi is achieved by loading a 2×2 AMC array on the back of the antenna, with a front to back ratio greater than 20 dB and radiation to the human body less than 0.15 W/kg. In [15], the antenna integrated with an AMC array achieved a maximum gain increase of 6.12 dBi while reducing backward radiation by 88.9%. In [16], the antenna and AMC array are printed on a substrate of FR4, which cannot adapt to the bending activity of the human body. Above antennas are all single element with AMC array, which greatly limits the channel capacity and information transmission rate of the communication system.

Multiple-input multiple-output (MIMO) technology has demonstrated its effectiveness in ensuring high data rates, enhancing system capacity, and reducing multipath fading. Isolation of the ports should be considered in the design of a MIMO antenna. High isolation means that there is little influence between antenna elements, and they do not interfere with each other when receiving and transmitting signals. In [17], a flexible MIMO antenna is presented, but the max

* Corresponding author: Chengzhu Du (duchengzhu@163.com).

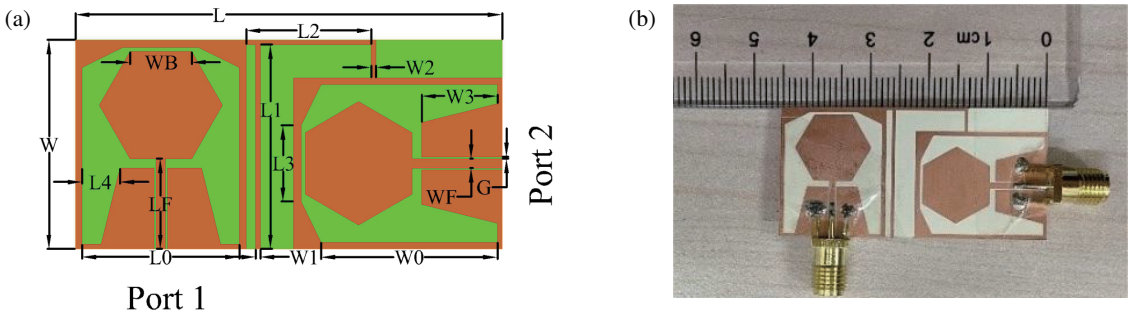

FIGURE 1. Design of MIMO antenna. (a) Geometry of MIMO antenna. (b) Manufactured MIMO antenna.

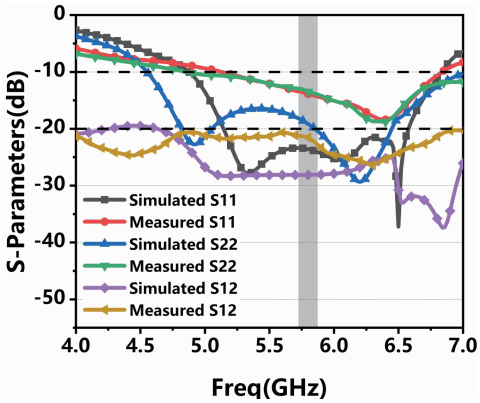

FIGURE 2. Simulated and measured S-parameters.

gain is only 5.5 dBi. In [18], a MIMO antenna with an AMC array is printed on a substrate of FR4, and the isolation is only -18 dB. So, it is a difficult task to design a fully flexible MIMO antenna based on an AMC array with high isolation and gain.

Based on the study of MIMO technology and AMC structure, a two-element MIMO flexible wearable antenna integrated 4×5 flexible AMC array is proposed, which improves the antenna gain and greatly reduces the backward radiation to human body. The substrate for both the AMC and the antenna is 0.1 mm flexible material LCP. The reflection phase and reflection bandwidth of AMC unit, the return loss of integrated antenna, the coupling between elements, gain, and normalized pattern are analyzed and discussed. At the same time, the SAR evaluation and bending measurement of the integrated antenna are carried out, and the results of measurement and simulation show a good agreement. The proposed antenna can be safely applied to human body and widely used in WBAN.

The innovation points of the proposed antenna include: (1) The MIMO antenna integrated with an AMC structure is fully flexible. (2) The MIMO antenna has high isolation.

2. DESIGN OF MIMO ANTENNA INTEGRATED WITH AMC

2.1. MIMO Antenna Design

The geometric dimensions of MIMO antenna are given in Fig. 1(a). The antenna is fed by coplanar waveguide, printed on a flexible liquid crystal polymer (LCP) material with a loss tangent of 0.002 and a relative permittivity of 2.9. The manufactured antenna is shown in Fig. 1(b).

By implementing angular processing on the ground, the operating frequency band of the antenna is expanded. Two antenna units are arranged vertically to avoid mutual coupling, and polarization diversity is utilized to improve isolation. The connected ground and isolated branches are introduced to further decrease coupling.

These are the detailed dimensions of MIMO antenna: $L = 45$ mm, $L0 = 16.6$ mm, $L1 = 21.5$ mm, $L2 = 13.2$ mm, $L3 = 8$ mm, $L4 = 4$ mm, $LF = 9.5$ mm, $W = 22$ mm, $W0 = 18.6$ mm, $W1 = 6.4$ mm, $W2 = 0.5$ mm, $W3 = 8$ mm, $WB = 6.5$ mm, $WF = 1$ mm, $G = 0.2$ mm.

The vector network analyzer is used for measuring the S-parameters of the antenna. A comparison of the S-parameters from simulation and measurement is depicted in Fig. 2. The simulated operating frequency band is 4.88 GHz–6.83 GHz, with isolation below -20 dB. Due to processing errors and practical measurement environment issues, the measured frequency range is narrower than the simulated bandwidth, ranging from 5.15 GHz to 6.8 GHz, with isolation less than -20 dB throughout the entire operating frequency band.

Figure 3 shows the design process of MIMO antenna with connected ground. Antenna 1 is the first step; Antenna 2 is the second step; Antenna 3 is the third step. As can be seen from Fig. 4, the introduction of ground connection and isolation branches enables the MIMO antenna to obtain good impedance

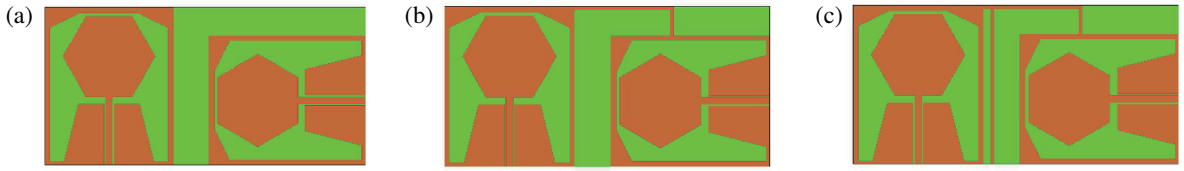

FIGURE 3. The design process of MIMO antenna. (a) Antenna 1. (b) Antenna 2. (c) Antenna 3.

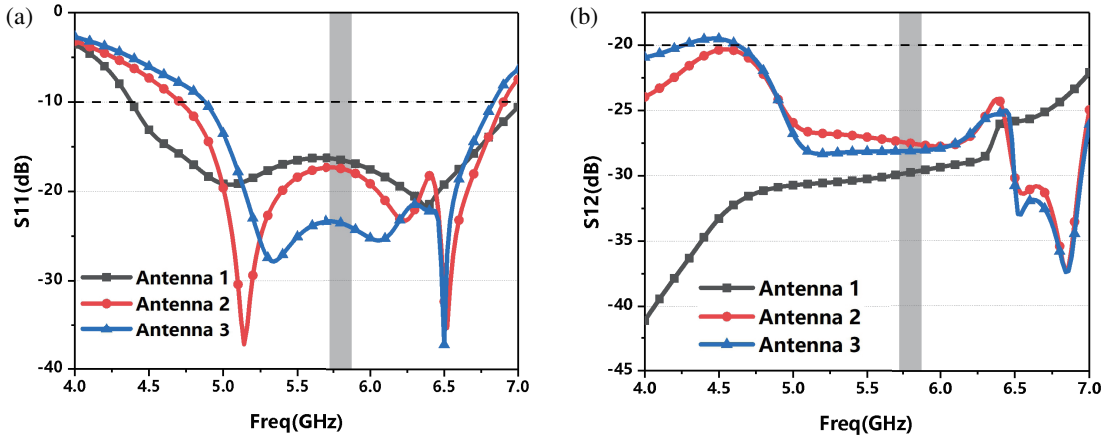

FIGURE 4. Simulated S-parameters (a) S_{11} (b) S_{12}.

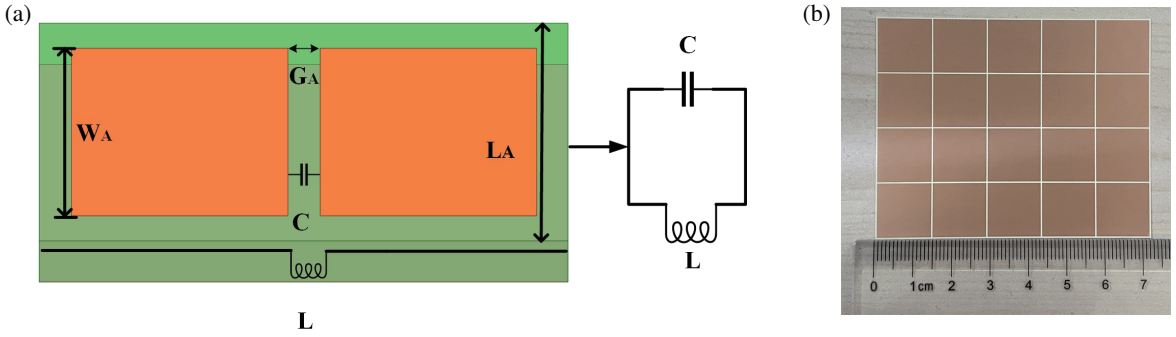

FIGURE 5. Design of AMC structure. (a) Equivalent circuit of AMC unit. (b) Manufactured AMC array.

matching and high isolation. At Industrial, Scientific, and Medical (ISM) 5.8 GHz, the return loss is less than -25 dB, and the isolation is better than 27 dB. The simulated operating frequency band is from 4.88 GHz to 6.83 GHz, and the isolation is less than -20 dB.

2.2. AMC Array Design

The front side of the AMC can be a conductive metal patch of any shape, and the back side is a complete metal ground connection, and periodically arranged on the substrate. The equivalent circuit of AMC structure is an LC parallel model. It can be seen from the resonance principle that the impedance of the LC parallel circuit is the maximum value in the resonant state, and the surface of the AMC presents high impedance characteristics. When the electromagnetic wave is vertically incident to the surface of the AMC structure, a part of the electromagnetic wave will be reflected. On the high-impedance surface, the incident wave and reflected wave are in phase and in positive superposition, so that the surface of the AMC presents in-phase reflection characteristics. The high impedance and in-phase reflection characteristics of the AMC can improve the gain and front-to-back ratio of the antenna.

The AMC unit is composed of a square patch on the front of LCP and metallic ground. The substrate is LCP with a thickness H_A of 0.1 mm. The unit length is L_A, and the length of the square patch is W_A. Fig. 5(a) shows the equivalent circuit of the AMC unit. The capacitor C is equivalent to the gap between the radiation patches, and the inductor L is equivalent to the ground [19]. The manufactured AMC array is shown in Fig. 5(b).

The center resonant frequency is 5.82 GHz, and the reflection phase bandwidth is 50 MHz (5.79 GHz–5.84 GHz). The reflection phase characteristics of the final optimized AMC are depicted in Fig. 6(a).

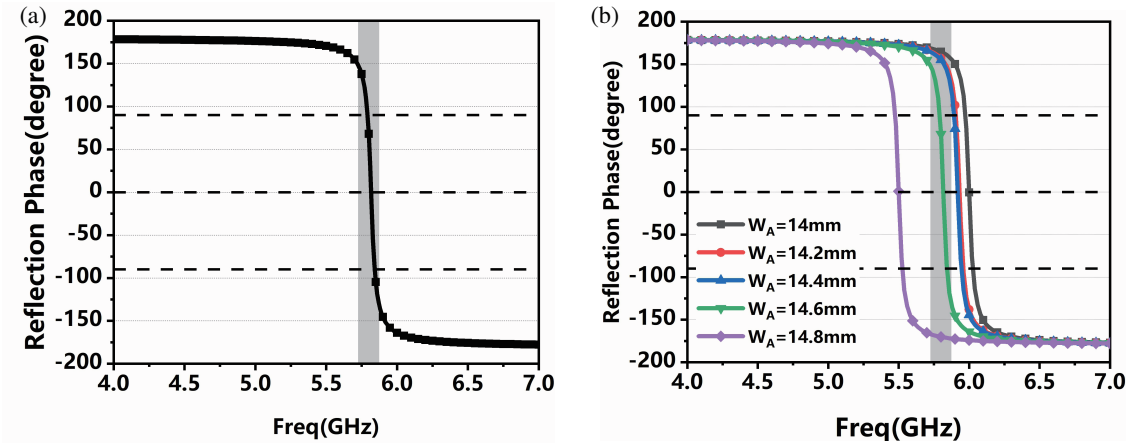

FIGURE 6. (a) Reflected phase of AMC. (b) Effect of W_A on AMC performance.

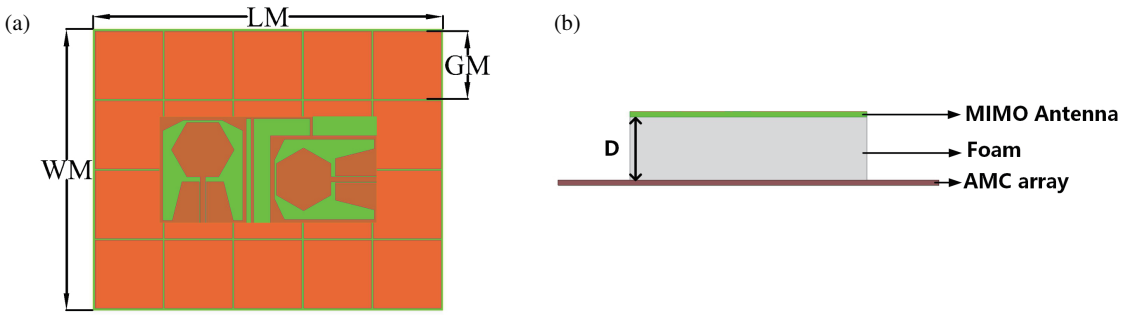

FIGURE 7. MIMO antenna integrated with AMC. (a) Top view. (b) Side view.

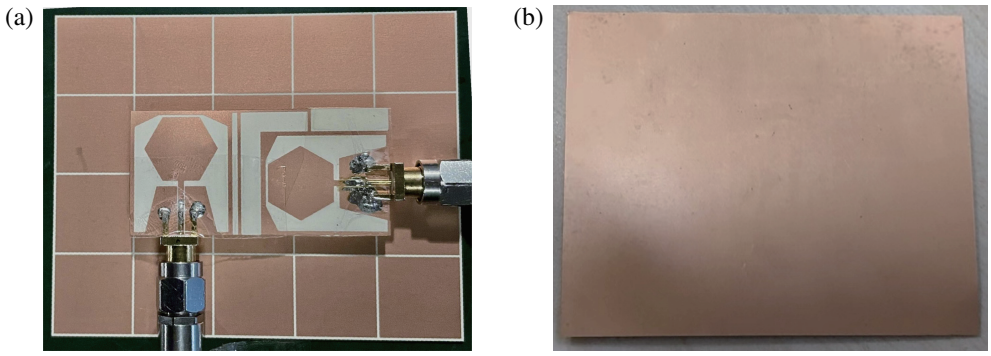

FIGURE 8. Manufactured integrated antenna. (a) Top view. (b) Side view.

The parameters of the AMC are analyzed, and the results are depicted in Fig. 6(b). As the W_A gradually increases, the 0° reflection phase of the AMC gradually shifts towards lower frequencies.

The detailed dimensions of the optimized AMC unit are given below: L_A =16 mm, W_A =14.6 mm, G_A =0.4 mm, H_A =0.1 mm.

2.3. MIMO Antenna Integrated with AMC Array

Figure 7(a) displays the MIMO antenna system integrated with a 4×5 AMC array. As shown in Fig. 7(b), the foam with a height of 12 mm is placed between the AMC array and the proposed MIMO antenna. The fabricated integrated antenna is shown in Fig. 8. Simulated S-parameters with different values of D are presented in Fig. 9.

As observed in Figs. 9(a) and (b), when the height of the foam is different, it has a significant influence on the S-parameters of the integrated antenna. Considering the performance of the integrated antenna and the low profile, a foam height of 12 mm is chosen.

The size of the AMC array also has an impact on the antenna gain, as shown in Table 1. With the increase of the number of AMCs, the antenna gain also improves. However, there is a diminishing effect on the antenna gain after reaching a certain

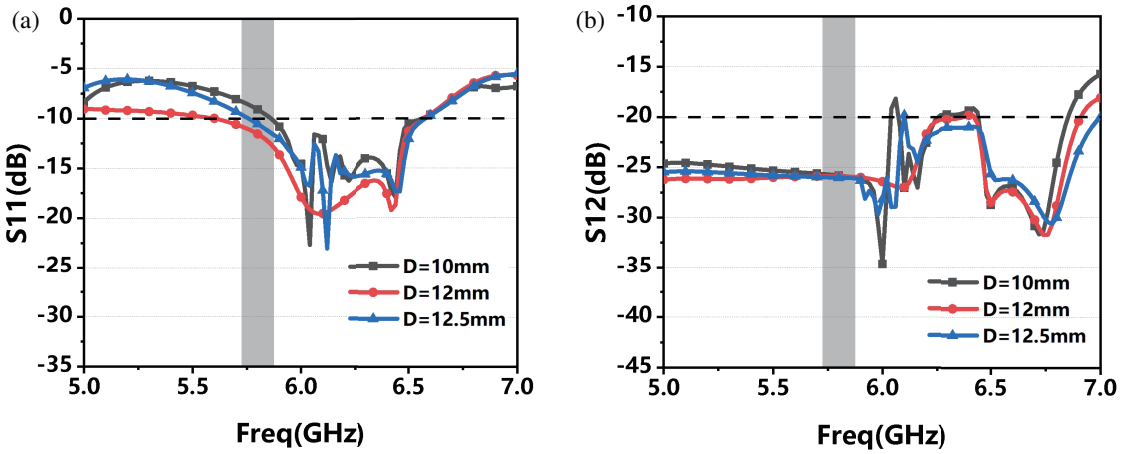

FIGURE 9. Effect of D on the performance of integrated antenna (a) S_{11}. (b) S_{12}.

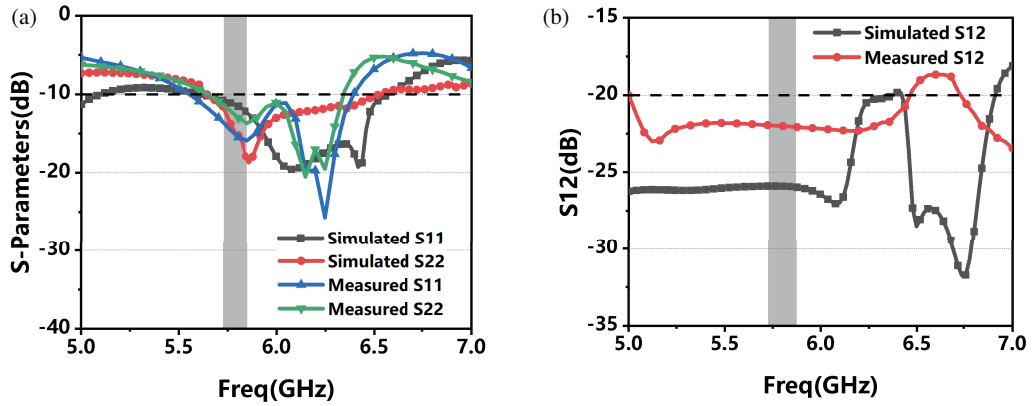

FIGURE 10. Simulated and measured S-parameters of proposed integrated antenna. (a) S_{11} and S_{22}. (b) S_{12}.

TABLE 1. Simulated gains of integrated antenna with different numbers of AMC array.

AMC Array Size	Gain (dBi)
3×4	8.28
4×4	8.6
4×5	8.8
5×5	8.7

quantity. Considering the performance and miniaturization requirements of the integrated antenna, a 4×5 AMC array is integrated on the back of the MIMO antenna to improve the overall performance.

To achieve a good match between the antenna and the AMC array, further simulated optimization is conducted for some dimensions of the AMC array, and the optimized dimensions are as follows: LM = 72.4 mm, WM = 58 mm, GM = 14 mm.

3. EXPERIMENTAL VERIFICATION

3.1. S-Parameters

The S-parameters of the integrated antenna from simulation and measurement are depicted in Fig. 10. It can be observed that the operating bandwidth of the integrated antenna is 5.6 GHz–6.68 GHz, with isolation less than -19.5 dB. The measured bandwidth of the integrated antenna is narrower, ranging from 5.55 to 6.4 GHz, and the isolation is less than -20 dB.

3.2. Diversity Performance

To guarantee optimal antenna performance, the envelope correlation coefficient (ECC), diversity gain (DG), and channel capacity loss (CCL) are analyzed [18]. The ECC should be as small as possible, which is preferably less than 0.5. The value of ECC can be calculated by the far field radiation:

$$\mathrm{ECC} = \frac{\left| \iint \left[\overrightarrow{F_1}(\theta,\varphi) \times \overrightarrow{F_2}(\theta,\varphi) \right] d\Omega^2 \right|}{\iint \left| \overrightarrow{F_1}(\theta,\varphi) \right|^2 d\Omega \iint \left| \overrightarrow{F_2}(\theta,\varphi) \right|^2 d\Omega} \quad (1)$$

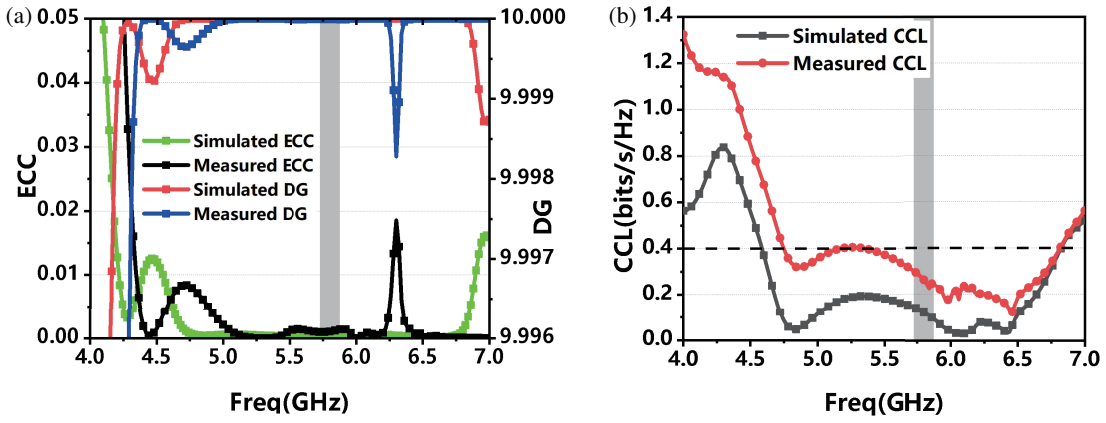

FIGURE 11. Simulated and measured ECC, DG and CCL of integrated antenna. (a) ECC and DG. (b) CCL.

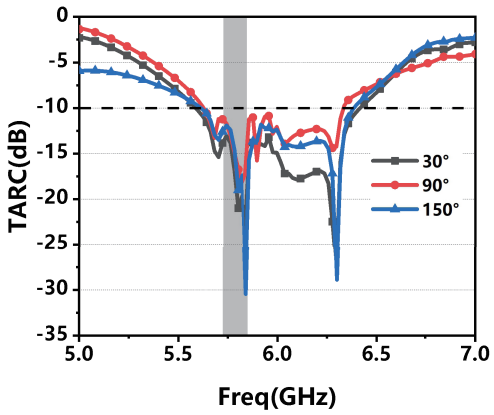

FIGURE 12. Measured TARC at different angles.

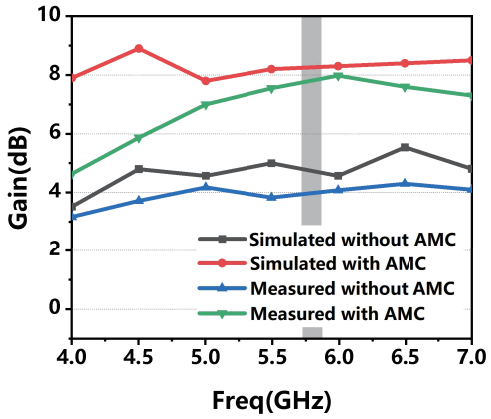

FIGURE 13. Simulated and measured gain of MIMO antenna without AMC and with AMC.

A higher DG indicates a better improvement in the effectiveness of diversity reception, as the difference in signal levels becomes larger. The CCL is a crucial index for assessing the dependability and transmission efficiency of channel. It is an important metric for assessing the performance of integrated antenna. The CCL can be calculated by (2) and (3):

$$\mathrm{CCL} = -\log_2 \det(a^R) \tag{2}$$

$$a^R = \begin{bmatrix} a_{11} & a_{12} & a_{13} & a_{14} \\ a_{21} & a_{22} & a_{23} & a_{24} \\ a_{31} & a_{32} & a_{33} & a_{34} \\ a_{41} & a_{42} & a_{43} & a_{44} \end{bmatrix},$$

$$a_{ii} = 1 - \left(\sum_{j=1}^{N} |S_{ij}|^2 \right),$$

$$a_{ij} = -(S_{ii}^* S_{ij} + S_{ij}^* S_{ij}) \tag{3}$$

Figure 11 shows the simulated and measured levels of ECC, DG, and CCL. At ISM 5.8 GHz, the ECC is less than 0.005, and the DG is greater than 9.999, approaching 10. The measured CCL is less than 0.4 bits/s/Hz. This indicates a low coupling between the antennas, a good diversity reception effect, and a small channel capacity loss.

The total active reflection coefficient (TARC) is another indicator that characterizes the performance of MIMO systems. It represents that the smoother the change of the antenna is at different angles, the better directivity and anti-interference ability are. It can be calculated by the following formula:

$$\mathrm{TARC} = N^{-0.5} \sqrt{\sum_{i=1}^{N} \left| \sum_{k=1}^{N} |sike^{j\theta k-1}| \right|^2} \tag{4}$$

Figure 12 analyzes the TARC of the integrated antenna and calculates the TARC of the integrated antenna at different angles of 30°, 90°, and 150°. At ISM 5.8 GHz, the TARC values are all below −10 dB. By analyzing the ECC, DG, TARC, and CCL, it is evident that the integrated antenna system has great performance.

3.3. Gain and Front-to-Back Ratio

The measured gain is increased from 4.02 dBi to 7.92 dBi as shown in Fig. 13. The simulated front-to-back ratio (FBR) of MIMO antenna is increased from 3.2 dB to 17.5 dB.

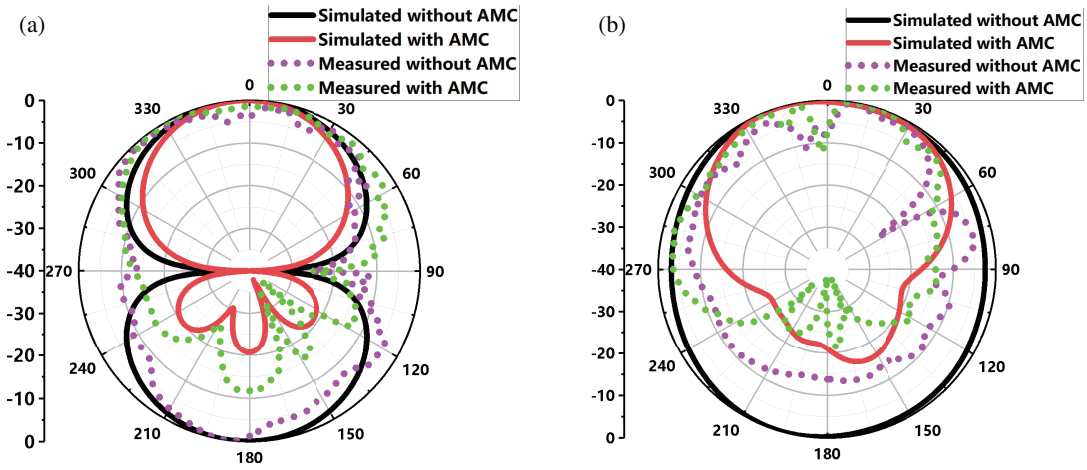

FIGURE 14. Simulated and measured patterns of integrated antenna. (a) E plane, (b) H plane.

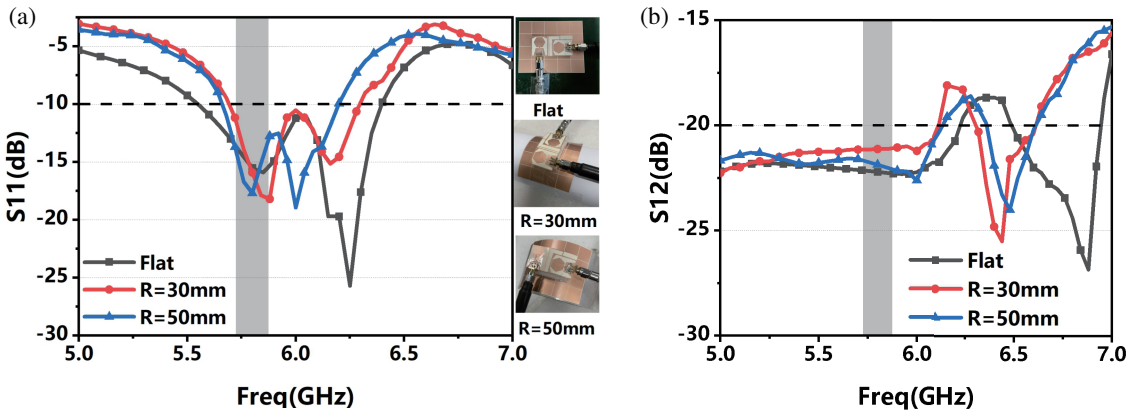

FIGURE 15. The S-parameters of bending measurements (a) S_{11} (b) S_{12}.

3.4. Radiation Patterns

In Figs. 14(a) and (b), the normalized radiation patterns of MIMO antenna without AMC array and with AMC array are analyzed in the E-plane and H-plane, respectively. In both the E-plane and H-plane, the integrated antenna exhibits reduced backward radiation.

3.5. Bending Analysis of Integrated Antenna

To verify the conformal capability of the integrated antenna, the antenna is placed on a cylinder with bending radii of 30 mm and 50 mm for measurement. The performance of the bending integrated antenna is displayed in Fig. 15. The measured results indicate that bending antenna has a narrow operating bandwidth and a shift towards higher frequency. With a bending radius of 50 mm, the operating frequency band is from 5.68 GHz to 6.2 GHz, with isolation better than 18.5 dB. With a bending radius of 30 mm, the operating band extends from 5.7 GHz to 6.28 GHz, with isolation below -18 dB within the operating frequency. The bending results demonstrate that the integrated antenna can still work normally under different degrees of bending, and the isolation meets the engineering requirements.

3.6. On-Body Effects on the Integrated Antenna

For evaluating the practical applicability of the proposed integrated antenna, we need to analyze the integrated antenna on the human body.

By incorporating human body analysis, we can assess the performance and safety of the integrated antenna when interacting with the human body.

Figure 16 shows the S-parameters of integrated antenna on human body. The integrated antenna is positioned independently on the human arm, thigh, and back for measurements. The measured operating bandwidths are 5.4–6.35 GHz, 5.65–6.4 GHz, and 5.64–6.36 GHz, with isolation below -19 dB. The high dielectric characteristic of the human body affects the working performance of the integrated antenna, making the working band of the integrated antenna narrow and the isolation worse. However, the measured operating bandwidths all cover ISM 5.8 GHz, with isolation below -20 dB. The results of the antenna measurements on the human body demonstrate that the antenna is applicable to WBAN.

In Fig. 17, simulated analysis is performed on the integrated antenna over four layers of human tissues [20]. These tissue structures include skin, fat, muscle, and bone.

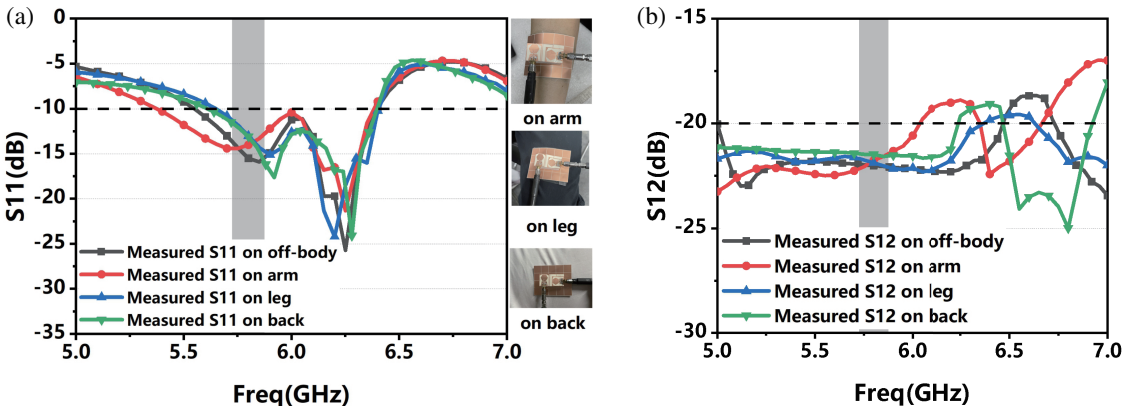

FIGURE 16. Measured S-parameters of integrated antenna on human body. (a) S_{11}. (b) S_{12}.

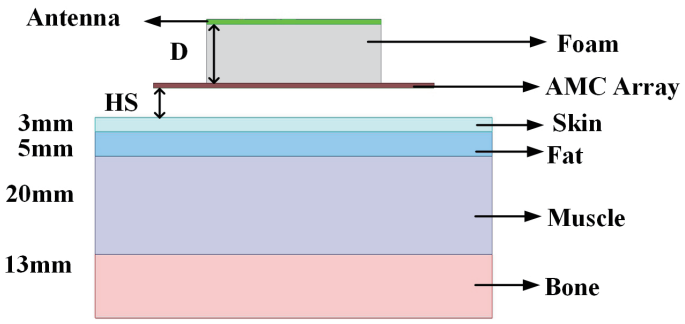

FIGURE 17. The simulated model of integrated antenna on human body.

TABLE 2. SAR comparisons of MIMO antenna with AMC and without AMC.

	HA	SAR (W/kg)
Without AMC array	2	4.25
	3	3.68
	4	2.85
With AMC array	2	0.09
	3	0.02
	4	0.017

TABLE 3. Comparison between the proposed antenna and other antennas.

Ref.	Number of elements	Substrate	Operating Frequency (GHz)	Gain (dBi)	Isolation (dB)	SAR (W/kg)
[8]	1	Textile Felt	2.37–2.45 (3%)	2.71	-	0.0091
[9]	1	Jeans fabric	2.3–2.5 (8%)	7.5	-	0.028
[10]	1	Polyester felt	2.38–2.6 (9%)	5	-	0.23
[11]	1	Jeans	2.16–2.48 (13%)	5.33	-	0.34576
[12]	1	Polyimide	2.42–2.46 (2%)	7.47	-	0.15
[13]	1	Leather	5.56–6.07 (8.8%)	7.47	-	
[14]	1	Felt	4.96–5.9 (16.2%)	6.7	-	0.2114
[15]	1	Pellon fabric	4.3–5.9 (27.5%)	6.12	-	1.32
[18]	2	FR4	2.36–2.51 (6.1%) 5.03–6.12 (18.8%)	3.34 7.48	< -18	0.16
This work	2	LCP	5.55–6.4 (14.6%)	7.92	< -20	0.09

According to U.S. and EU regulations, respectively, the SAR values obtained by the antenna with an AMC structure remain below the threshold at 2 W/kg/10 g, which ensures the safe application of the concerned antenna for wearable purposes [21]. It can be calculated using the following formula:

$$\mathrm{SAR} = \frac{\sigma E^2}{\rho} \tag{5}$$

ρ represents the mass density, E the electric field intensity, and σ the conductivity of human tissue.

The simulation of integrated antenna near the human body is analyzed by High Frequency Structure Simulator (HFSS). When the input power is 0.1 W, the SARs of the integrated antenna at different heights from the human body are displayed in Table 2. Compared to the MIMO antenna without AMC array, the radiation of the integrated antenna to the human body is significantly reduced. When the integrated antenna system is separated from the human body at different distances, the SAR values are all less than 0.09 W/kg, and the backward radiation to the human body is small, which all meet the EU standards.

4. PERFORMANCE COMPARISON

Table 3 presents a comparison between the proposed antenna and wearable antennas integrated with AMC in recent years. Compared with the wearable single antennas in [8–15], the presented antenna has more element than others. Compared with the MIMO antenna in [18], the presented MIMO antenna is flexible and has higher isolation. Table 3 illustrates that the proposed flexible MIMO antenna integrated with AMC array in this paper exhibits high gain, low SAR, high isolation, and ease of conformity. Its excellent flexibility and performances make it suitable for wearable applications.

5. CONCLUSION

A flexible wearable MIMO antenna system with an AMC array is proposed in this paper. The results of measurement and simulation show a good agreement. The AMC array is integrated on the back of the antenna, and the operating frequency band is 5.55 GHz–6.4 GHz (14.6%); the isolation is better than 20 dB; the measured gain at 5.8 GHz is 7.92 dBi, which increases by 3.9 dBi; and the SAR is less than 0.09W/kg. The results of simulation and measurement illustrate that the MIMO antenna system has the characteristics of high gain, low SAR value, and high isolation, and the flexibility makes the proposed antenna widely used in the wearable field. At the same time, the study provides a research direction for the future development of wearable MIMO antenna. A compact and wide-band wearable flexible MIMO antenna backed on an AMC array will be designed for low SAR, high gain, and high information transmission rate.

REFERENCES

[1] Ashyap, A. Y. I., S. H. B. Dahlan, Z. Z. Abidin, M. I. Abbasi, M. R. Kamarudin, H. A. Majid, M. H. Dahri, M. H. Jamaluddin, and A. Alomainy, "An overview of electromagnetic band-gap integrated wearable antennas," *IEEE Access*, Vol. 8, 7641–7658, 2020.

[2] Ali, U., S. Ullah, B. Kamal, L. Matekovits, and A. Altaf, "Design, analysis and applications of wearable antennas: A review," *IEEE Access*, Vol. 11, 14 458–14 486, 2023.

[3] Rana, M. R. and M. B. Hossain, "Design and performance enhancement of triple band antenna using metamaterial superstrate for wireless communications," in *Proceedings of the 6th International Conference on Electrical, Control and Computer Engineering*, 1117–1127, 2022.

[4] Youssef, O. M., M. E. Atrash, and M. A. Abdalla, "A compact fully fabric I-shaped antenna supported with textile-based AMC for low SAR 2.45 GHz wearable applications," *Microwave and Optical Technology Letters*, Vol. 65, No. 7, 2021–2030, Jul. 2023.

[5] Zheng, H., W. Cui, R. Liu, Z. Li, C. Fan, M. Wang, and E. Li, "Design of flexible dual-band antenna and metamaterial structure for wearable body area network," *International Journal of RF and Microwave Computer-Aided Engineering*, Vol. 32, No. 5, e23083, May 2022.

[6] Hazarika, B., B. Basu, and A. Nandi, "An artificial magnetic conductor-backed monopole antenna to obtain high gain, conformability, and lower specific absorption rate for WBAN applications," *International Journal of RF and Microwave Computer-Aided Engineering*, Vol. 30, No. 12, e22441, 2020.

[7] Nie, H.-k., X.-w. Xuan, and G.-j. Ren, "Wearable antenna pressure sensor with electromagnetic bandgap for elderly fall monitoring," *AEU — International Journal of Electronics and Communications*, Vol. 138, 153861, 2021.

[8] Kareem, F. R., M. E. Atrash, A. A. Ibrahim, and M. A. Abdalla, "All-textile inspired-folded dipole antennas for on/off-body communications medical applications," *Alexandria Engineering Journal*, Vol. 61, No. 11, 8751–8761, Nov. 2022.

[9] Ashyap, A. Y. I., Z. Z. Abidin, S. H. Dahlan, H. A. Majid, and G. Saleh, "Metamaterial inspired fabric antenna for wearable applications," *International Journal of RF and Microwave Computer-Aided Engineering*, Vol. 29, No. 3, e21640, Mar. 2019.

[10] Yao, L., E. Li, J. Yan, Z. Shan, X. Ruan, Z. Shen, Y. Ren, and J. Yang, "Miniaturization and electromagnetic reliability of wearable textile antennas," *Electronics*, Vol. 10, No. 9, 994, 2021.

[11] Naganathan, S. B. T. and S. Dhandapani, "Solar cell integrated wearable patch antenna on artificial magnetic conductor for on-body and in-body communications," *Applied Computational Electromagnetics Society Journal*, Vol. 37, No. 5, 576–587, May 2022.

[12] Yin, B., J. Gu, X. Feng, B. Wang, Y. Yu, and W. Ruan, "A low SAR value wearable antenna for wireless body area network based on AMC structure," *Progress In Electromagnetics Research C*, Vol. 95, 119–129, 2019.

[13] Saha, P., D. Mitra, and S. K. Parui, "Control of gain and SAR for wearable antenna using AMC structure," *Radioengineering*, Vol. 30, No. 1, 81–88, 2021.

[14] Gao, G.-P., C. Yang, B. Hu, R.-F. Zhang, and S.-F. Wang, "A wearable PIFA with an all-textile metasurface for 5 GHz WBAN applications," *IEEE Antennas and Wireless Propagation Letters*, Vol. 18, No. 2, 288–292, 2018.

[15] Alemaryeen, A. and S. Noghanian, "On-body low-profile textile antenna with artificial magnetic conductor," *IEEE Transactions on Antennas and Propagation*, Vol. 67, No. 6, 3649–3656, Jun. 2019.

[16] Aitbar, I., N. Shoaib, A. Alomainy, A. Quddious, S. Nikolaou, M. A. Imran, and Q. H. Abbasi, "AMC integrated multilayer wearable antenna for multiband WBAN applications," *Computers, Materials and Continua*, Vol. 7, No. 2, 3227–3241, 2022.

[17] Zhang, J., C. Du, L. Pei, and H. Liu, "A CPW-fed dual band four-port MIMO antenna based on liquid crystal polymer for flexible IoT applications," *International Journal of Microwave and Wireless Technologies*, Vol. 15, No. 9, 1570–1578, 2023.

[18] Du, C., L.-R. Pei, J. Zhang, and C.-X. Shi, "A gain enhanced dual-band low SAR AMC-based MIMO antenna for WBAN and WLAN applications," *Progress In Electromagnetics Research M*, Vol. 115, 21–34, 2023.

[19] Abu, M., M. Muhamad, Z. Zakaria, and H. Hasan, "Millimeter-wave parasitic AMC patches on the array antenna," in *2016 International Conference on Computer and Communication Engineering (ICCCE)*, 19–24, Kuala Lumpur, Malaysia, 2016.

[20] Gao, G., S. Wang, R. Zhang, C. Yang, and B. Hu, "Flexible EBG-backed PIFA based on conductive textile and PDMS for wearable applications," *Microwave and Optical Technology Letters*, Vol. 62, No. 4, 1733–1741, Apr. 2020.

[21] Bouamra, W., I. Sfar, A. Mersani, L. Osman, and J.-M. Ribero, "Design of a textile AMC-backed antenna for wearable applications," in *2022 Microwave Mediterranean Symposium (MMS)*, 1–5, Pizzo Calabro, Italy, 2022.